Preliminary Steps in Developing Rapid Aero Modeling Technology

Patrick C. Murphy,[1] David B. Hatke,[2] Vanessa V. Aubuchon,[3]
Rose Weinstein[4], Ronald C. Busan[5]
NASA Langley Research Center, Hampton, VA, 23681

The Rapid Aero Modeling (RAM) approach is a method to efficiently and automatically obtain aerodynamic models during testing, significantly saving time and resources. Motivation for this technology results from demand for experimental efficiency and model fidelity that has increased with growing aircraft complexity and aerodynamic nonlinearities. These issues are typical in the responses presented by a class of vehicles categorized as Urban Air Mobility aircraft where many features from both airplane and rotorcraft are present. For UAM configurations, with typically many more factors than conventional aircraft, traditional test methods can lead to increased costs and missed interactions. RAM guides the test to obtain high-fidelity, statistically rigorous aircraft models, and the approach is applicable to computational, ground, or flight-test experiments. It combines concepts from Design of Experiment theory and Aircraft System Identification theory that allow the user the freedom to choose, in advance of the test, a specific level of fidelity typically, in terms of prediction error. RAM only collects data required to meet the user-specified fidelity and fidelity is only limited by the facility and test article capabilities. An initial wind tunnel test to support development of RAM was conducted to assess potential metrics, algorithms, and procedures. This paper presents results from initial tests for the development of RAM technology and highlights some of the unique features of RAM applied to a conventional configuration during a ground-based, static, wind-tunnel test.

I. Nomenclature

B_i	=	regression coefficients
C_N	=	normal force coefficient
C_m	=	pitching-moment coefficient
$\bar{c}$	=	mean aerodynamic chord, ft
R^2	=	coefficient of determination
x_i	=	regressors
y	=	response variable in regression equation
α	=	angle-of-attack, deg
β	=	sideslip angle, deg
ε	=	error in regression model
σ	=	standard error

[1] Senior Research Engineer, Dynamic Systems and Control Branch, MS 308, Associate Fellow.
[2] Research Engineer, Flight Dynamics Branch, MS 308, non-member.
[3] Assistant Branch Head, Flight Dynamics Branch, MS 308, Associate Fellow.
[4] Pathways Student, Flight Dynamics Branch, MS 308, Student Member.
[5] Senior Research Engineer, Dynamic Systems and Control Branch, MS 308, Member.

II. Introduction

Aerodynamic modeling is a key part of the aircraft development process, particularly for new vehicle designs. Under the Transformational Tools and Technologies Project, NASA is recognizing the need for development of state-of-the-art computational and experimental tools and technologies required for development and prediction of future aircraft performance. Areas where future aircraft are being advanced with increasing interest are in Urban Air Mobility (UAM), distributed electric propulsion, and electric vertical take-off and landing configurations. Market studies supported by NASA highlight the opportunities and difficulties for these areas both in terms of economics and technology [1-2].

While the new design space offers significant opportunities, it also creates vehicles with substantially more complex and nonlinear aerodynamic responses, as well as increased complex interactions among propulsion and aerodynamic control systems [3]. Depending on the design stage being considered, varying levels of fidelity, and in turn, varying levels of resources are required. Even in early design stages for UAM vehicles where lower fidelity may be sufficient, the presence of rotors, props, wings, and fuselage results in a greater number of factors to consider, thus, contributing to significant design complexity. This can limit the ease of design changes while advancing through various design stages. Although advances in computer technology have facilitated more effective tools to tackle these issues, obtaining greater model fidelity still requires a significant investment of engineering time and resources both analytically and experimentally. A number of research efforts to improve fidelity and efficiency have been made in ground-based testing [4-12], flight testing [13-17], and in computational methods [18-25]. The authors are also supporting current research by NASA in the UAM area [26-30].

A unique approach to improving the modeling process by reducing the adverse impacts described above is through development of a testing process called Rapid Aero Modeling (RAM). RAM capitalizes on fundamentals from design of experiment (DOE) and aircraft system identification (SID) theory. In addition to automating the modeling process, it offers an opportunity for significant savings in time and resources. This study highlights the initial development of the RAM process that provides statistically rigorous results and limits the amount of data collected to that needed to achieve user-defined levels of fidelity. For this study, fidelity levels are defined by model prediction errors. It is important to note that maximum fidelity is always limited by the accuracy and measurement capabilities of the test apparatus and physical model under test. RAM is under development for application to wind tunnel environments (RAM-T) and application to computational environments (RAM-C).

In this paper, preliminary results for RAM-T are presented. Consideration is given to potential metrics, algorithms, and procedures that can allow the RAM process to be implemented. Two experiments were performed on a conventional, off-the-shelf, radio-controlled model aircraft. The model, referred to as the "Mini-E," is shown in Fig. 1.

Figure 1. Conventional aircraft configuration (Mini-E) in LaRC 12-Foot Low Speed Tunnel.

The first experiment was a conventional static test designed to obtain basic aerodynamic characteristics over a large flight envelope. The objectives were two-fold: (1) obtain sufficient data to support a simulation suitable for flight dynamics and controls studies, and (2) provide conventional data for comparison with the second experiment. The second experiment was designed to evaluate candidate procedures and metrics that might support a RAM-T process in a static-test application. In the latter case, the focus was primarily on the longitudinal axis with sweeps in sideslip

limited to +/- 5 degrees. One aspect of RAM-T to be tested was whether the sequential process envisioned would be able to produce models with prediction errors less than 3%. This paper highlights results and lessons learned from application of two different approaches to aerodynamic modeling based on static testing in a wind-tunnel facility: (1) a conventional approach providing a traditional basis for comparison and (2) assessment of a non-conventional approach using components of RAM-T technology.

III. Aerodynamic Modeling Methods

Conventional testing in wind tunnels has a long history and well-established practices that have been demonstrated and corroborated through comparisons with flight test and computational methods. This approach typically involves a fairly controlled environment where one-factor-at-a-time (OFAT) methods are used to sweep over one of the states or controls for the vehicle under test while all other factors are held constant. Statisticians will disagree with the OFAT approach due to the possibility of unknown systematic errors being confounded with the data; however, practitioners go to great lengths to ensure that at least known systematic errors minimized or eliminated. Conventional techniques also seem to work well for cases where the number of factors are limited to just traditional control surfaces and propulsion systems. For modern UAM designs, the number of factors can be anywhere from three to five times the number of traditional factors. This quickly degrades a conventional experiment design from capturing all possible factor interactions as well as higher-order nonlinearities in any practical manner or time frame. This is especially true when time and resources are limited. RAM-T, rooted in SID and DOE best practices, offers a solution that can significantly ameliorate these problems. The underlying theory in SID and DOE is well established in academia, industry, and government for a variety of applications. SID has roots progressing from Gauss (1809), Fisher (1912), to Kalman (1965), while credit for the initial development of DOE is often given to Fisher [31]. DOE has since expanded and modernized from Fisher's agricultural applications to all fields of modern science and engineering. Application of RAM-T and RAM-C to new UAM designs with combined airplane and rotorcraft features is a current area of research.

A. Model Identification

Aerodynamic modeling can be accomplished in a number of ways depending on the specific goals of the investigator. A commonly used process for obtaining aircraft aerodynamic models using aircraft SID is shown in Fig. 2. This process is well documented in Ref. [32]. Several methods can be applied for each block in this flow chart;

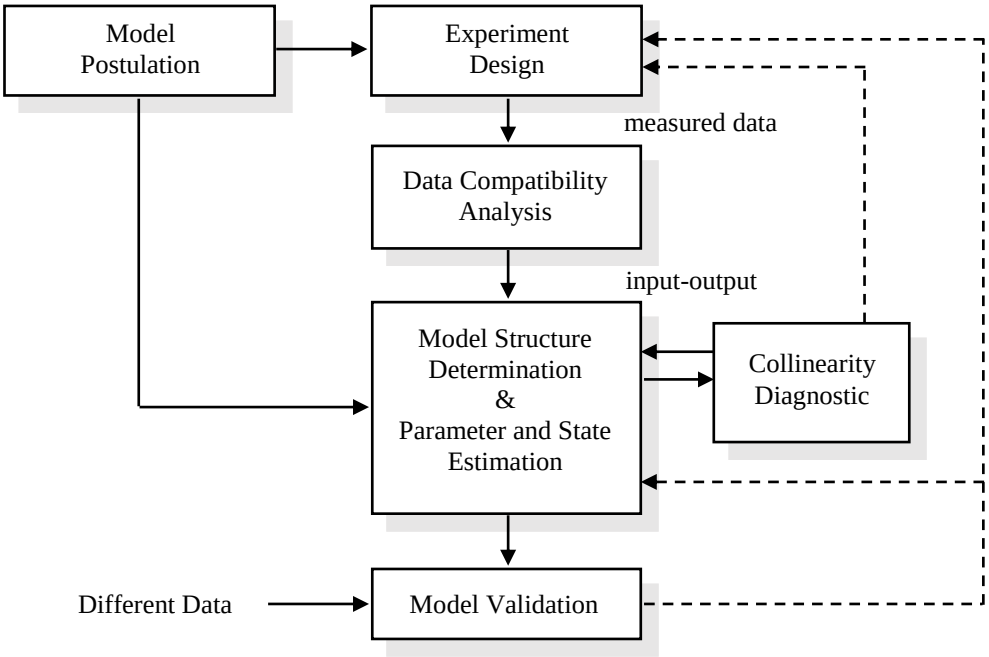

Figure 2. Aircraft system identification process.

however, for the RAM-T process, two key blocks are accomplished differently from common practice. The first difference is in the top block, labeled Experiment Design, and the second is in the bottom block, labeled Model

Validation. In general the top block captures many key aspects of the experiment, including test conditions, motions or maneuvers, instrumentation, and specification of required measurements. In this study DOE methods will be applied to achieve these same goals. Closely tied to this step is the Model Postulation block, where decisions on the allowable model structures and any a priori knowledge about the system dynamics can influence where in the flight envelope testing is performed as well as the type of maneuvers required for the test. After measurements are collected, an important step is to ensure data compatibility. This analysis is done, particularly for flight experiments, using kinematic relationships to remove any systematic errors (usually in the form of bias and scale factors) that might be present in the measurements. The next step is Model Structure Determination where the model form is estimated from within the previously postulated class of model structures. For this study, polynomials are used as the basic mathematical form for all aerodynamic models. Given a set of input-output measurements containing sufficient information content and a representative model structure, a number of parameter estimation techniques are adequate to determine the unknown parameters in the model with acceptable accuracy. For this study, stepwise regression is used where the model structure and parameter estimation steps are combined. Stepwise regression facilitates a very efficient adjustment of the model as data are obtained. A practical concern, as part of the parameter estimation process, is assessing the degree to which model terms may be correlated. Although some degree of correlation is often present, proper experiment design and model structure can limit this issue. Experiment designs based on DOE techniques can be expressly designed for this purpose. The last major step in SID is Model Validation, which is a test of the model performance against data not used for estimation. This step provides verification that the estimated model is a good predictor of the dynamic system responses within acceptable error bounds.

B. DOE Application for RAM Development

In advance of performing any experiment, DOE theory provides guidance on setting up an efficient and statistically rigorous test plan. Experiment design based on DOE is well documented in Ref. [33]. In this study DOE is applied to wind-tunnel testing to obtain a static aerodynamic model; however the aerodynamic model is a test case to allow development of the RAM process. The primary objective is to develop techniques suitable for an automated RAM-T process that capitalizes on the benefits of DOE principles. This was done by manually exercising prototype RAM logic and assessing the possible metrics and procedures that might be best suited for an automated RAM-T. In particular, key principles of blocking and the sequential nature of DOE testing facilitates an automated process. Five basic principles commonly used in DOE design are:

1. Orthogonal regressors – uncorrelated regressors to improve estimation calculations.
2. Replication – independent and repeated measurements to assess system noise and uncertainty.
3. Randomization – randomized input matrix to average out extraneous factors and unknown systematic errors.
4. Blocking – technique to improve precision and reduce variability due to known nuisance factors.
5. Sequential testing – a knowledge building process that allows each step to benefit from the previous one.

Ideal test facilities are automated and allow replication and randomization to support DOE-based experiments. The ability to command any position of the model, test rig, and model actuators from a pre-defined user test matrix, followed by recording of input commands, achieved set points (verified by measurements), and aerodynamic responses is ideal. Feedback control that ensures accurate set points is important for repeatability and ensuring regressors achieve their orthogonal design characteristics. Blocking must be incorporated by design to remove the effects of known sources of error (nuisance variables) and easily applied in an ideal test facility.

Experimentation is an iterative process that, depending on a priori knowledge, may require a series of initial tests such as screening experiments to determine important factors or, more commonly in aerospace applications, exploratory experiments to determine the location or presence of certain aerodynamic features. Other reasons such as envelope expansion or limited test times can lead to a planned series of tests. Sequential testing simply reflects application of the scientific method, and fortunately, DOE designs are sequential in nature and seamlessly promote the scientific method.

The foundation for DOE classical designs is the factorial experiment [31]. A factorial design is one which varies all factors simultaneously for all possible combinations. Using two levels for each factor represents a run-efficient method for developing a first order plus interaction model. A full-factorial design in two factor space is shown below in Fig. 3 with the addition of a center point.

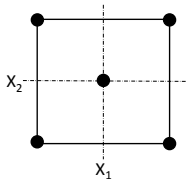

Figure 3. A full-factorial design in two-factor space.

Replicated centers afford a test for possible augmentation to support quadratic model terms. This type of information allows the investigator to sequentially build models and only incorporate increasing amounts of data as required. The supported regression model is shown with up to two-factor interactions (2FI) by

$$y = B_0 + \sum_i B_i x_i + \sum \sum_{i \neq j} B_{ij} x_i x_j + ... + \varepsilon \quad i = 1, 2, ..., k \tag{1}$$

The B_i, B_{ij}, are the fitted regression coefficients and the x_i are the factors (independent variables or regressors). A refinement (augmentation) to the factorial design is the central composite design (CCD) [34] which adds design points along the axes through the origin of the design space as shown by the square symbols of Fig. 4.

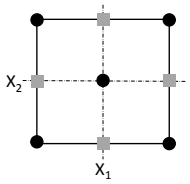

Figure 4. A face-centered central composite design in two-factor space.

This approach supports a full second order model given in Eq. (2).

$$y = B_0 + \sum_i B_i x_i + \sum_i B_{ii} x_i^2 + \sum \sum_{i \neq j} B_{ij} x_i x_j + \varepsilon \quad i = 1, 2, ..., k \tag{2}$$

The location of the axial points defines this CCD as a face-centered design (FCD). The nested face-centered design allows the nesting of two FCD designs to support the addition of pure cubic terms to the empirical model. The two FCD's may be tuned by fractionating the factorial designs as presented by Landman et al. in Ref. [7]. The design in two-factor space is shown in Fig. 5

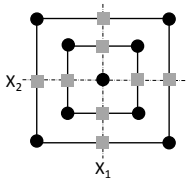

Figure 5. A nested face-centered design in two-factor space.

where the supported model is given by Eq. (3).

$$y = B_0 + \sum_i B_i x_i + \sum_i B_{ii} x_i^2 + \sum \sum_{i \neq j} B_{ij} x_i x_j + \sum_i B_{iii} x_i^3 + \varepsilon \quad i = 1, 2, ..., k \tag{3}$$

Sets of DOE designs in this study were developed as sequences of five blocks. After the nested face-centered design, a series of I-optimal blocks are used. Examples are shown in section IV-C. Blocking served two purposes: first, the sequence of smaller data collection blocks reduced miscellaneous nuisance bias errors, such as from different

tunnel operators, different days of operations, and tunnel overheating during long runs; second, the sequence allowed model analysis to be performed and evaluated against validation data to either confirm testing was complete or to indicate additional data were required. When a validation failure occurs, indicating additional data are required, it is an indication that either the progression to higher-order models is needed or specific regions must be further investigated. Validation tests assessing prediction-error residuals readily highlight when and where the prediction error is failing to meet user benchmarks.

C. Validation Tests for RAM Development

Validation tests are part of the SID process, shown at the bottom block in Fig. 2. To avoid confusion with related terms used by different disciplines, the term validation will be used to identify tests performed on data not used for model identification. These tests provide confirmation that the estimated models represent the aerodynamic model under test to within some pre-defined acceptable fidelity. For this study, acceptable fidelity is quantified by prediction error applied to validation data. Acceptable fidelity and accuracy for non-dimensional aerodynamic coefficients can depend on a number of factors, including the purpose the aerodynamic models will serve. A tradeoff is always made between model fidelity, precision, speed, and cost limitations.

A practical method for assessing validation is to observe the residuals between measured and predicted responses. For well-designed experiments that result in adequate models, the residuals appear as white noise with magnitudes generally within the specified acceptable levels. Not every residual test point will meet the acceptable error boundary limit. As described in Ref. [35], success or failure of a given test point residual to meet the requirement can be judged as a binomial experiment. For example, theoretically, the expectation for a coin toss is that out of 100 tosses of a fair coin, 50 heads and 50 tails will occur. However, in a practical experiment that exact ratio of ½ tails or heads is extremely unlikely to occur. The number of successes and failures relative to the expected value can be modeled as a binomial distribution and therefore the number of allowed failures can be defined based on the number of trials in the validation experiment. For a 100 coin toss experiment, the critical binomial number is 42, given a 50% probability of success that the residual was within tolerance, at a 95% confidence level. After running a coin toss experiment, if less than 42 heads (or 42 tails) occurred then one could infer that the coin did not have a 50% probability of landing on heads with no more than 5% inference error. For RAM development, the number of residuals considered is typically 75, and consequently the critical binomial number is typically 66 given a 95% probability of success that the residual is within tolerance. This is computed at a 99% confidence level, implying up to a 1% inference error.

The validation step is possibly the most important step in the SID process. Typically experimentalists collect more data than needed in an effort to drive down model fitting statistics, such as standard deviation or correlation coefficients, but this is misleading since the estimation process (often regression) is by definition minimizing the error at test points. This approach does not directly improve prediction error tested on non-regression points. However, a number of useful metrics can be used to aid in that process. Predicted Residual Error Sum of Squares (PRESS) and Predictive Squared Error (PSE) are commonly used metrics and are presented herein with Bayesian Information Criteria (BIC) as candidate metrics. BIC is a penalized likelihood function that assesses the likelihood of the fitted model being correct while penalizing over-parametrization. PRESS is determined by computing the prediction error sum of squares where each residual error is computed without that particular data point included in the model. PSE provides a penalty to PRESS when terms are added to the model.

Three objectives need to be satisfied in order to collect the correct amount of data: (1) minimize standard error to get an adequate model fit, (2) minimize prediction error to get a useful model, and (3) only collect enough data to meet the precision, prediction, and validation requirements. These objectives will reflect a balance among the precision demanded by the experimentalist, the capabilities or precision levels possible by the test apparatus, and the time and cost required to meet those demands. The basic goal is to expand data collection only enough to meet the model complexity requirements.

In the experiment design phase, the investigator must define the confidence level required, signal/noise ratio for the test apparatus, and the minimum level of response detection required. However, in the execution phase, the investigator must also pre-define a level of acceptable prediction error for validation tests in order to confirm an adequate model and to prevent over-collecting data. Data and model complexity are inherently connected. Collecting more data or adding more terms to a model are not necessarily steps to a better model. Designs in section IV will show that simply doubling the amount of data can degrade the variance inflation factor (VIF), indicating the regressors can suffer reduced orthogonality. Experimental results in section V demonstrate potential model degradation with increasing number of model terms or model complexity.

IV. Test Plans for Modeling Experiments

Designing experiments for this study covered two distinct purposes. The first was to develop a test plan that would provide sufficient aerodynamic data to support simulation development for flight dynamics studies and experimental control law development. The second purpose was to develop a plan that would provide preliminary results to guide RAM-T development. The intent of running these two tests in sequence was to provide some corroborating evidence that RAM-T provided comparable results.

A. Facility and Model Details

The Langley 12ft Low-Speed Tunnel (12-ft LST) facilitated preliminary development of the RAM testing method. The 12-ft LST[*] is an atmospheric pressure, open circuit tunnel enclosed in a 60-foot diameter sphere. The test section is octagonal with a width and height of 12 feet and a length of 15 feet with each octagonal side measuring 5 feet. The maximum operating pressure is q = 7 psf (V = 77 ft/sec at standard sea level conditions), which corresponds to a Reynolds number of approximately 492,000 per foot. The longitudinal center-line-flow in the test section has a turbulence level of about 0.6 percent. Test section airflow is produced by a 15.8-ft. diameter, 6-blade drive fan powered by a 280 HP, 600 volts, 600 RPM DC motor which is controlled by a 500 HP AC motor that drives a field controlled generator. The 12-ft LST is operated from its control room positioned behind the test section and the drive fan. The model can be observed through the large viewing windows or the multiple controllable video cameras.

The model was mounted on a 6-axis balance and connected to the tunnel's C strut via a belly-mounted sting. The C Strut allows the attitude of the model to be controlled by the data acquisition system. This system was connected to an Arduino mega via a UDP connection. The Arduino was mounted in the model and commanded one servo on each of the 7 control surfaces. The Arduino sent a pulse width modulation (PWM) command to each servo. It also recorded the actual angular position of the surfaces via 7 encoders, which was then reported back to the data acquisition system. This system removed the need to manually change the position of a control surface between runs. The commanded PWM signals for each servo and encoder output were calibrated from measurements taken at a minimum of 5 different angular positions. With this system, a run file of the desired model attitude and surface deflection at each data point was able to be loaded into the data acquisition system. The data acquisition system would then command all the needed changes during the run and capture all of the data recorded for the run and report it in a single file. The types of data recorded include, the 6 forces and moments on the model, the commanded and actual positions of the surfaces, the angle of attack and sideslip of the model, and the flow conditions of the tunnel.

The model aircraft used in these tests was a radio controlled (RC) hobbyist kit consisting primarily of aircraft plywood and balsa structure overlaid with a MonoKote film. Researchers recognize that RC hobbyist hardware used for wind tunnel testing commonly needs to be strengthened to handle the higher loading produced by the wind tunnel. RC hobbyist airframes are designed to handle the loads they will see in flight, where the stresses through the structure are typically limited by the reaction forces produced by the vehicle inertia. An airframe mounted on a wind tunnel sting or post will often produce stresses through the structure that are much higher.

To help ameliorate this problem, the hobbyist kit was modified by adding aluminum structure (4 parallel rails with intermittent cross members) extending from the motor mounts back through the aft fuselage, and graphite rods extending from the mid fuselage back to the area where the horizontal and vertical stabilizers attach. In addition to stiffening the fuselage/empennage structure, the aluminum rails also provided attachment points for the balance block and sting post required to mount the model in the tunnel. The wings, horizontal and vertical tails, and all the individual control surfaces were deemed strong enough that they would not break during wind tunnel testing. However, it was clear they would undergo significant deflection under load. Eliminating the deflection issue would require remaking all these main vehicle components and control surfaces from stiffer materials. This was not an acceptable option due to cost and schedule impacts. The effect of surface flexibility on modeling and benefits of the structural modifications are discussed in section V-A.

B. Conventional Test Plan

The conventional wind tunnel test plan was developed to meet the two objectives highlighted previously – to build an aerodynamic database and to guide RAM-T development. The test occurred in the 12-Ft LST at a dynamic pressure of 2 psf while varying angle of attack, angle of sideslip, and control surface deflections. The test space is summarized in Table 1. The difference in factor ranges considered between two approaches to testing are noted.

[*] https://researchdirectorate.larc.nasa.gov/12-foot-low-speed-tunnel-12-ft-lst/

Table 1. Factor ranges for conventional and DOE tests

No.	Label	Description	Low	High	Units	Notes
			Range	Range		
1	α	Angle of attack	-6 -5	36 35	deg deg	Conventional test DOE test
2	β	Sideslip	-30 -5	30 5	deg deg	Conventional test DOE test
3	LA	Left aileron	-30	30	deg	Both tests
4	LF	Left flap	-30	30	deg	Both tests
5	RF	Right flap	-30	30	deg	Both tests
6	RA	Right aileron	-30	30	deg	Both tests
7	LE	Left elevator	-30	30	deg	Both tests
8	RE	Right elevator	-30	30	deg	Both tests
9	RUD	Rudder	-30	30	deg	Both tests

The test outline included a model and system shake-down to ensure that all equipment was working properly and that the data was adequate. In order to identify interesting non-linear regions in the aerodynamics, a fine α-schedule sweep was performed. Nominal α- and β-schedule sweeps were also conducted at select α's and β's. The effect of the flaps, elevator, rudder, and ailerons were also observed, as well as the interactions of control surfaces. The system was unpowered for the duration of the test. Power effects will be captured in a future test. The test matrix, showing baseline runs, control surface sweeps, DOE baselines with a reduced angle-of-attack range, and control surface interactions, is shown in Fig. 6.

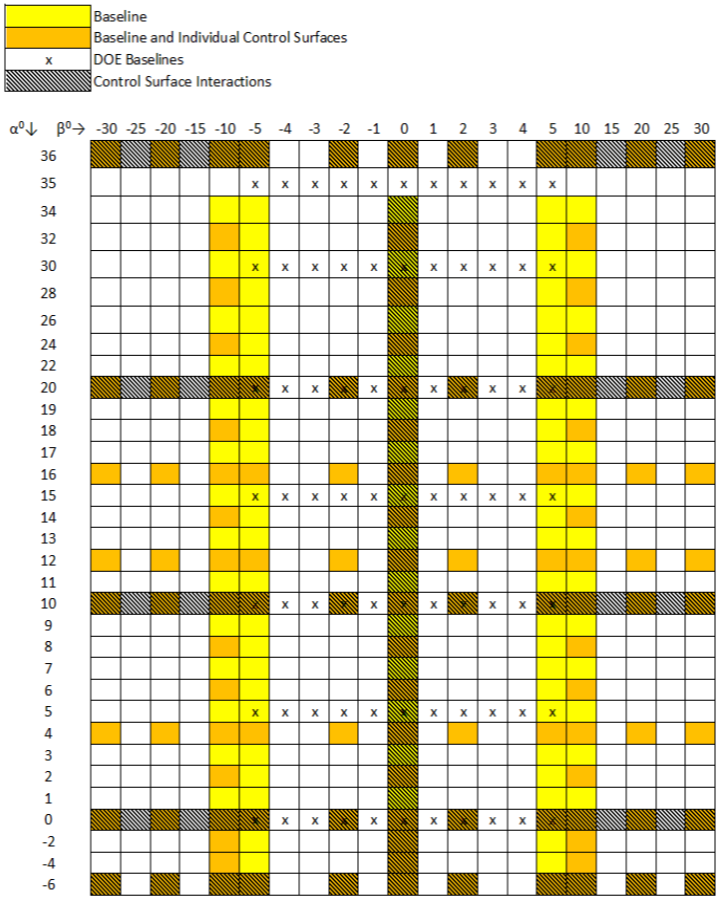

Figure 6. Conventional wind tunnel test matrix.

C. RAM Development Test Plan

In the RAM development test plan, a series test blocks were designed to reflect a sequence of obtaining data as needed to model progressively more complex models. In a RAM progression the test only moves forward if more complex models are required to meet prediction-error requirements and, consequently, more data are required to support higher-order polynomial modeling. For this study only 5 DOE blocks were designed in advance, however, the number and size of blocks needed can change with different applications. The size of each block can be adjusted for a number of reasons, for example, experience indicates that tunnel overheating can occur for blocks that are too large and run too long.

Table 2 shows several design metrics used for each block. The first is the variance inflation factor (VIF) that reflects the degree of orthogonality for the regressors. Values of VIF are equal to one if regressors are perfectly orthogonal. Values over 10 reflect a degradation of orthogonality in certain regressors and may require further design evaluations. Fraction of Design Space (FDS) is a graphic tool for evaluating the standard error profile. The number reflects the fraction of the design space within the expected variance parameters. For the design process, an assumption is made that standard deviation is 1 to allow relative predictive error to be computed. For this evaluation a very conservative assumption is made that the signal-to-noise ratio is only 2. The last metric indicates the experimental power (to avoid type 2 errors) for which values over 80% are commonly seen as acceptable.

Maximum values of the design metrics shown in Table 2 were selected from a survey of all model terms to show how each block design was progressing and improving the overall design as blocks of additional design points were added. The first three of five blocks present a sequence of designs: FCD, nested FCD, and I-optimal that define the primary test sequence. I-optimal designs are based on minimizing the integrated prediction variance over the design space. Each block was designed assuming a full quadratic model and each step provided more degrees of freedom for a more complex model, if needed.

The VIF values in block 2 show the cost of adding a nested FCD in order to capture potential nonlinearities as expressed in Eq. (3). The nested FCD is particularly useful in aerospace applications to handle nonlinear responses due to control surface deflections, and it ensures the full range of each surface is covered. The third block is an I-optimal design that minimizes prediction error. This block strategically added 222 runs and brought all the design metrics to excellent levels. The first three blocks were expected to be sufficient for modeling the aerodynamic coefficients, especially in the lower angle-of-attack region below stall, where models were expected to be almost linear or mildly quadratic. Blocks 4 and 5 provided either validation data or additional modeling data if model complexity demanded even higher order terms and in turn required a larger amount of data. The optimal blocks are useful for validation data since the optimizer avoids using existing design points. Block 4 is also shown applied to both quadratic models and cubic models. The degradation to the experiment design of adding block 4 to the cubic case is relatively small since the FDS metric, the preferred metric for response surface modeling, is still satisfactory. Although in an automated RAM process not all blocks may be needed, in this case, all the blocks were run to provide additional insights into the entire modeling process.

Table 2. Maximum (worst case) values of design metrics (9 Factors)

Block Type	Blocks	Runs	Design Terms	VIF	FDS	% Power
	(inclusive)					2σ, s/n=2
Minimum Resolution V FCD	1	70	Quadratic	6.72	0.81	80.0
Nested FCD	1, 2	140	Quadratic	10.60	0.95	86.3
I-optimal	1, 2, 3	362	Quadratic	1.53	1.0	99.9
*Mixed (I-opt)	1, …, 4	437	Quadratic	1.46	1.0	99.9
*Mixed (I-opt)	1, …, 4	437	Cubic	25.19	1.0	85.4
Validation (I-opt)	1, …, 5	512	Cubic	24.85	1.0	91.7

*Block 4 can be used for validation or, if needed, provide data for more complex models.

Figure 7 presents the nine-factor, full angle-of-attack range, three-block design, viewed as a function of angle of attack and sideslip. The graphic shows the basic FCD (red squares, partially hidden), the nested FCD (green squares), and the I-optimal points (blue squares). Similar plots of design points are obtained by plotting any two of the nine factors.

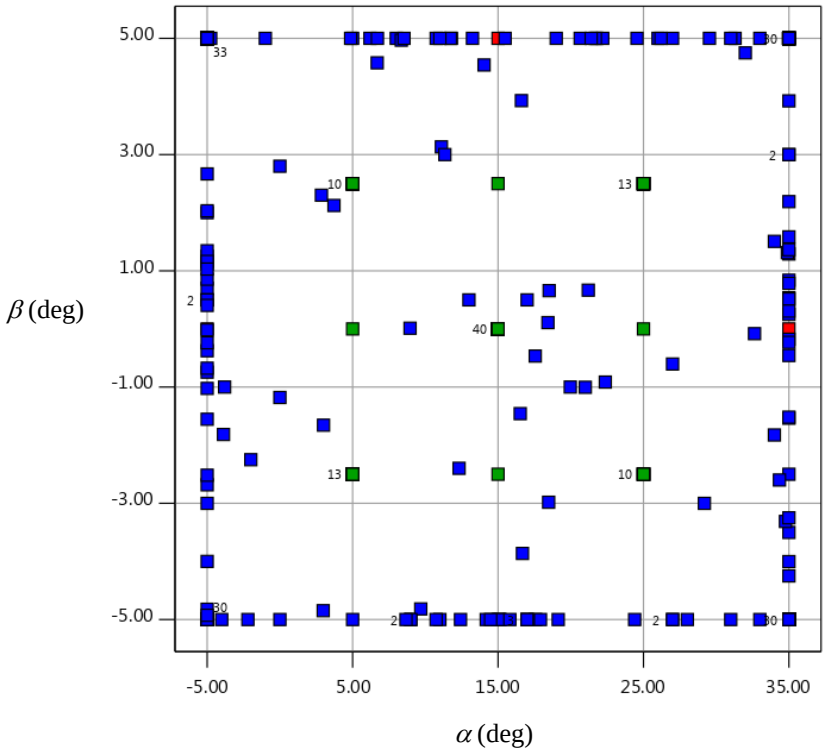

Figure 7. DOE design for three blocks: FCD (red), Nested FCD (green), and I-optimal (blue).

At the start of the test, full ranges for all the factors were defined. During the test, if all 5 blocks of data are still insufficient to meet the pre-defined fidelity levels, then the test ranges can be adjusted to smaller regions. The selection of smaller regions is a current area of research [28]; however, in the RAM process the selection of regions would depend on where the offending prediction-error results occur. For this preliminary study without the automated RAM system in operation, a selection had to be made in advance. The choice for this study was to simply split the regions in terms of angle of attack until a satisfactory prediction error was obtained. The choice of angle of attack to determine regions reflects the dominant role it plays in aerodynamic response. Figure 8 shows the sequence used in this study. The widest region with the largest factor ranges is labeled as R1. The split of R1 results in R2 and R3, and so on.

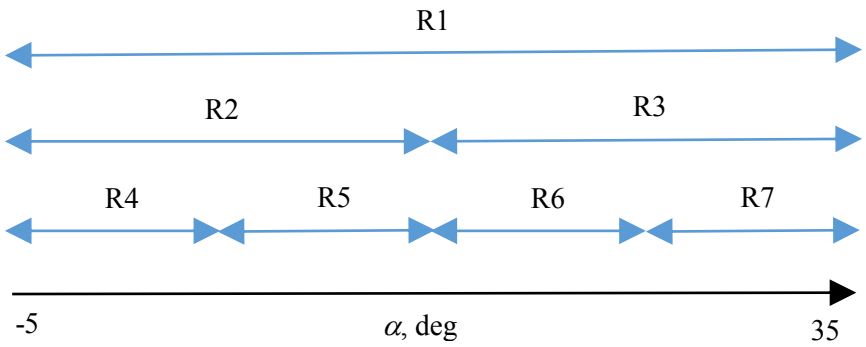

Figure 8. RAM test-region splits.

Additional efficiencies occur in an automated RAM process by virtue of the splitting process. Once data is collected for a region to be split, the sub-regions already have a substantial amount of data required for that new region. There is no need to repeat the full data collection process for each new sub-region.

After development of the progressive DOE blocks and splitting test regions, the overall operation of an automated RAM process is more tractable. The general RAM concept is presented in Fig. 9 as a simplified flow chart. On the

left is the user-desired level of model fidelity and a set of designed experiments appropriate for the vehicle under test. As the test facility processes each block to produce measurements for model identification, the resulting Analysis of Variance (ANOVA) tables characterize the relative significance of model terms and other sources of variation. Effectively, the RAM process provides a control loop around the vehicle under test that guides the test through a series of data blocks that are used to estimate models and evaluate their performance. The series of data blocks takes advantage of the sequential nature of designed experiments and only requests more data if it is needed for either estimating a higher-order model or for more detailed investigation in a region where model performance is inadequate. The test is completed when model validation tests are passed, indicating the requested level of fidelity is achieved, or the test may conclude when the limits of the test apparatus measurement capabilities are reached. The choice of identification methods, prediction error metrics, or how the test regions are split is not restricted by the RAM-T process. As mentioned in the introduction, this process can also be applied to a computational "facility" as well.

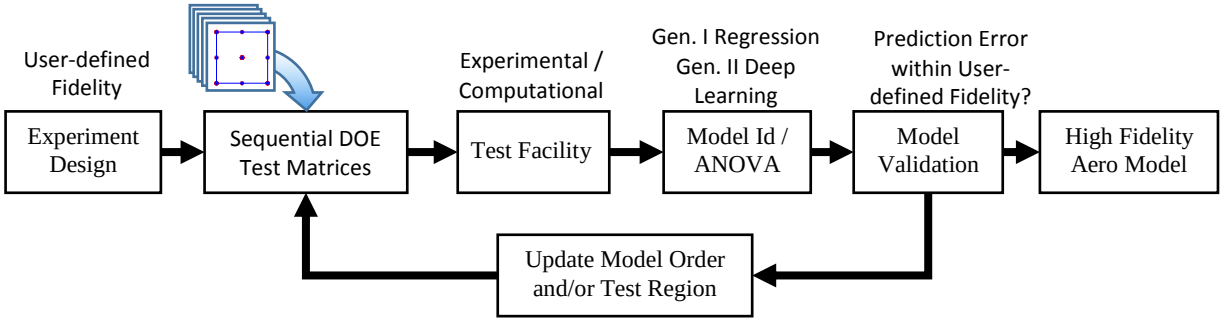

Figure 9. RAM process.

Since this study was not an automated closed-loop RAM-T test, an approximation of the process is reflected in the test plan to allow evaluation of the methodology. To focus the discussion, only longitudinal-force coefficients are considered for the detailed progress evaluations of RAM-T. However, the final models for all 6 coefficients are presented in section V-C.

From previous testing in the 12-ft LST with physical models meeting tunnel standards, the general expectation is to achieve 3% - 5% prediction error for aerodynamic models of the normal force coefficient. Errors less than 3% define the desired level of fidelity but 5% is acceptable and still represents an adequate model. In this study the purpose was to test experiment design approaches using an inexpensive radio-controlled class model and actuators in a relatively short test program. Some of the issues associated with testing lower-precision aircraft test articles are discussed in the next section. However, testing a higher fidelity model was not necessary to achieve the RAM development objectives. Consequently for this study, acceptable prediction errors could be relaxed.

V. Experimental Results

In this study, results from two approaches to aerodynamic modeling are considered. The first set of results, for the conventional approach, produce basic aerodynamic characteristics and comparison data for the second approach. As mentioned previously, the second approach was investigated primarily to assess potential testing procedures, metrics, and algorithms for development of the RAM-T approach.

A. Conventional Test Results

Aerodynamic models from conventional tests are often used to produce data look-up tables (in the form of increments) for simulation software and to display trends against key states that reveal important stability and control characteristics. Sample aerodynamic characteristics of the Mini-E are highlighted in this section, and the appendix presents a more complete set of results. At the design center-of-gravity location, the aircraft is both longitudinally and lateral-directionally stable. The longitudinal aerodynamics and static stability are shown in Fig. 10. The pitching moment curve shows that the airplane is longitudinally stable for the aircraft's flight center-of-gravity location. The lift curve is approximately linear below stall and shows that the aircraft exhibits a very gentle stall beginning about α = 12 degrees.

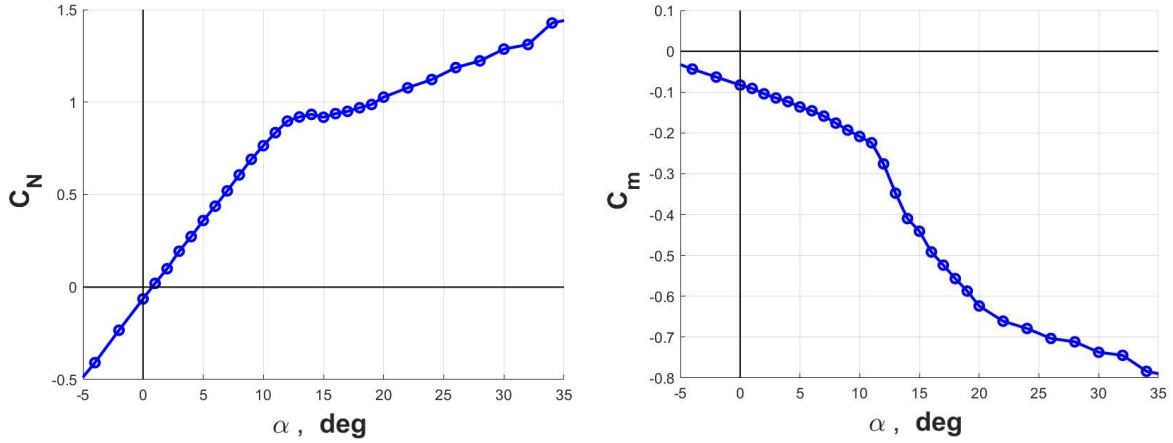

Figure 10. Longitudinal aerodynamics.

The effects of model flexibility, described in section IV-A were monitored during testing. As anticipated, the control surfaces exhibited significant flexing under aerodynamic loads, in particular at high angles of attack and at large magnitude commands. As a result, set-point error existed between the commanded and measured control surface signals. The additional stiffening structure added to the servo mounts for each elevator at the beginning of testing improved these errors substantially but not completely. Standard deviations for the set-point errors varied among the surfaces. As an example, standard deviations for the left and right elevators are shown in Table 3. The right elevator standard deviation was reduced by 80% while the left elevator improved by 20% based on block 1 models of the surfaces commanded and measured performance.

Table 3. Standard Deviations, σ, for elevator set-point errors

	LE	RE
Before stiffening	1.41	2.29
After stiffening	1.17	0.48

Comparing the commanded control surface values with the encoder measurements for each surface during the tests revealed the remaining systematic error present in the tests. For example, Fig. 11 illustrates this phenomenon for the LE with commands of 10° and 30° during two angle-of-attack sweeps at zero sideslip. Several options exist for reducing this source of error:

1. More extensive rebuild of model structures to achieve desired level of stiffness.
2. Add feedback control to ensure commanded positions are achieved.
3. Develop and apply new calibration functions to reflect dependency on angle of attack.
4. Use measured surface values instead of commanded values.
5. Accept the error as an additional source of systematic error during testing.

For this study, the level of fidelity required was relatively low, so less time and resources were considered for options 1 and 2. Feedback control was used, however, for moving the test rig and setting angle-of-attack and sideslip angles. Consequently, standard deviations for alpha set-point errors were on the order of 6.0×10^{-05} deg, with similar values resulting for sideslip. Options 3 and 4 are easily incorporated into the modeling process but option 3 would require a redesign of the experiment using the new calibration information. Option 4 is the easiest to apply and the preferred choice for cases where options 1-3 are not possible; however, this choice reflects some degradation in the optimized experiment. Option 5 was chosen for this study with the realization that although randomization can help to ameliorate many sources of systematic error, the resulting models will still reflect greater prediction error due to the mismatch between commanded and achieved surface positions. Set-point error is an issue for any modeling option since the range for the affected factor is not fully realized in the experiment.

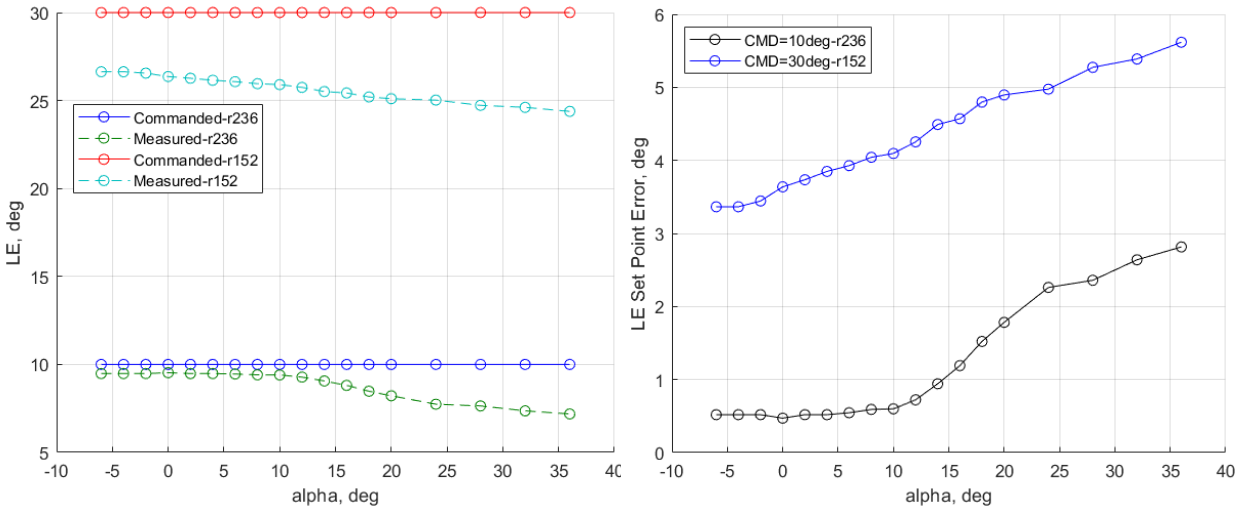

Figure 11. Set-point error due to flexible control surfaces.

B. RAM-T Development Results

In this study the objective was to manually process the steps that an automated RAM-T process might follow, determine best procedures, and note any issues that might present obstacles for this approach. Metrics that can support modeling decisions during data processing are shown in Table 4. The table shows an example of a variety of statistical metrics for the C_N coefficient models estimated during a sequential test described in Table 2. Progression through blocks 1-4 using data from region R1 is accomplished using stepwise regression. Block 5 is retained strictly for validation tests. Polynomial models were identified for each of the six cases shown in Table 4, and reflect increasing model complexity going from case 1 to case 6. The "Design model," "Model form," and "No. of terms" rows show the type of DOE design, type of polynomial, and corresponding number of polynomial terms, respectively. Model terms were selected using stepwise regression where the confidence level for parameter entry and exit into and out of the polynomials varied in order to consider cases with varying numbers of terms. However, confidence levels for the final models are estimated at 95%.

Table 4. DOE test metrics: modeling progression for blocks 1-4.

case #	1	2	3	4	5	6
block #	1	1	1	2	3	4
Design model	FCD	FCD	FCD	Nested FCD	I-Optimal	I-Optimal
Model Form	Linear + 2FI	quadratic + 2FI	cubic + 3FI	cubic + 3FI	cubic + 3FI	cubic + 3FI
No. of terms	8	22	54	41	67	68
No. of runs	70	70	70	140	362	437
R^2	0.9157	0.9992	1.0000	0.9962	0.9977	0.9976
Adj R^2	0.9062	0.9988	0.9999	0.9947	0.9971	0.9972
Pred. R^2	0.8994	0.9984	0.9993	0.9928	0.9966	0.9967
Std. Dev.	0.2485	0.0280	0.0097	0.0460	0.0403	0.0408
Mean	0.5879	0.5879	0.5879	0.5879	0.5879	0.5983
C.V.%	42.27%	4.76%	1.65%	6.71%	6.69%	6.81%
PRESS	4.57	0.0750	0.0304	0.3917	0.6973	0.8391
PSE	0.57	0.0034	0.0006	0.0096	0.0104	0.0123
BIC	29.23	-235.0	-324.1	-307.5	-968.1	-1202.3
**e_i/C_Nmax %	14.69%	7.1%	8.6%	6.8%	4.4%	4.4%

**residual e_i = C_N_measured – C_N_predicted, $C_N$max = 1.7538

Cases 1-3 only consider the first block of data to allow some features of the metrics to be displayed. It should be noted that model statistics characterize the benefits of model improvements from adding terms to the model based on a given data set. When new blocks of data are added, the baseline for the evaluation metrics changes making direct comparisons difficult and requires some caution. Considering only cases 1-3 for block 1 data shows that increasing the model complexity improves all of the metrics except for the prediction error metric at the bottom. Metrics with penalties for additional terms will not continue to improve by adding more terms. Consistency across all cases is realized for the prediction error metric at the bottom of Table 4, since it is computed based on residuals using only block 5 validation data. Residuals (computed as measured-predicted values) are normalized by the largest value of the coefficient being modeled to form this prediction error metric. The values shown reflect the smallest errors that satisfy a binomial test described in section III-C. Since prediction error is still larger than desired, progress to additional blocks of data is indicated.

The FCD design for block 1 supports Eq. (2), which is a quadratic model with 2-factor interactions. Since results from block 1, case 2, do not provide satisfactory prediction error results, it is necessary to progress to a more complex model. More model complexity, in this case a cubic expansion of the polynomial, requires more data to support it. This highlights the rationale and benefits of a sequential approach to modeling. At this point it is appropriate to add block 2 data, a nested FCD, which provides a minimum set of data for a cubic model structure. To highlight the rationale of not simply increasing the complexity of the model without adding more data, case 3 is included in Table 4. Case 3, with a polynomial model including cubic and 3-factor interactions terms, shows improvements in a number of metrics except for a slight worsening of prediction error. Figure 12 presents residual plots to demonstrate the seeming contradiction in results. This is a common occurrence in modeling and highlights the need for validation data. Improvement in fit residuals are a result of the test data being regressed upon and fitting better as the model is made more complex with more terms. The validation data, which has not been regressed upon, reflects the true prediction capability of the model being tested.

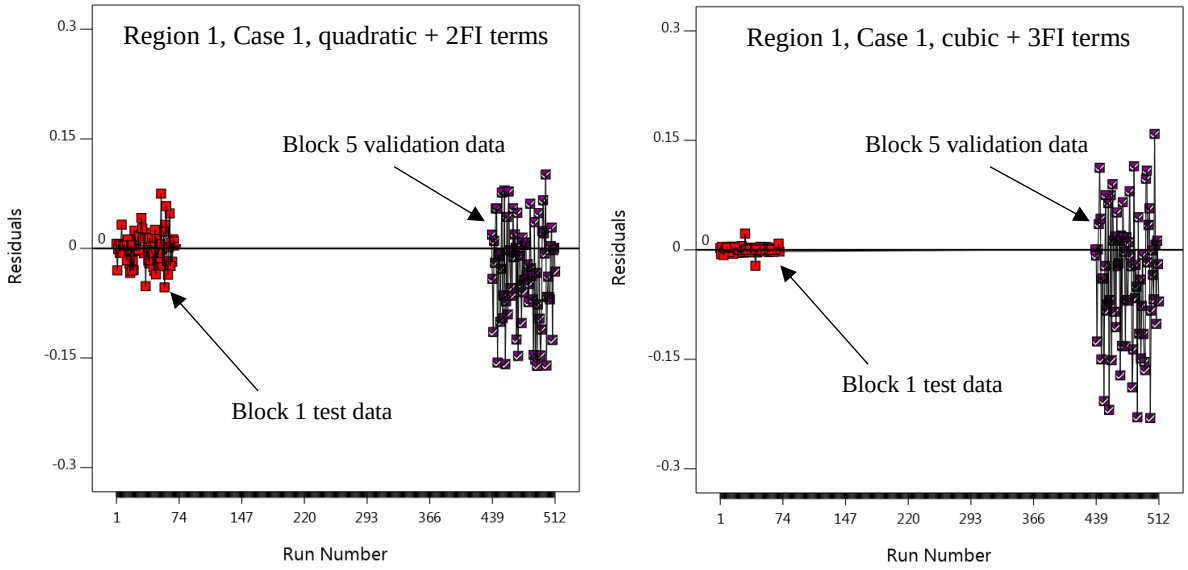

Figure 12. Impact of regression on test and validation data for two polynomial models.

Case 4 shows the benefit to adding block 2 data and allowing a more complex model but the model still cannot meet the desired prediction error benchmark. Case 5 shows the desired predictive model is achieved while the penalty metrics are flattening, indicating modeling progress should stop. Case 6 confirms there is no advantage to adding this additional data for the prediction error as well as showing some additional degradation in the penalty metrics.

The last step in the identification process for region R1 is checking the model against validation data. The key metric was shown at the bottom of Table 4. Figure 13 shows model and validation residuals for case 6, which is the last model for the analysis. Validation points, shown as block 5, are indicated by check mark in the data point symbol. For this model, only 9 validation points fail to meet the 4.3% error bound resulting in the claim that the model satisfies the acceptable prediction error requirements of 5%. This criterion is based on the critical binomial number for 75 test

points, where 66 successful points out of 75 are required to claim the residuals are within tolerance, given a 95% probability of success and no more than 1% inference error. The residuals show no trends during the experiment and present as a white noise process indicating no other variables or processes are confounded with the data. The occasional large residual likely reflects the lower-quality physical model used in this study. Included in the graphic are the 4.3% of maximum-range error bounds that show the prediction error achieved for this test.

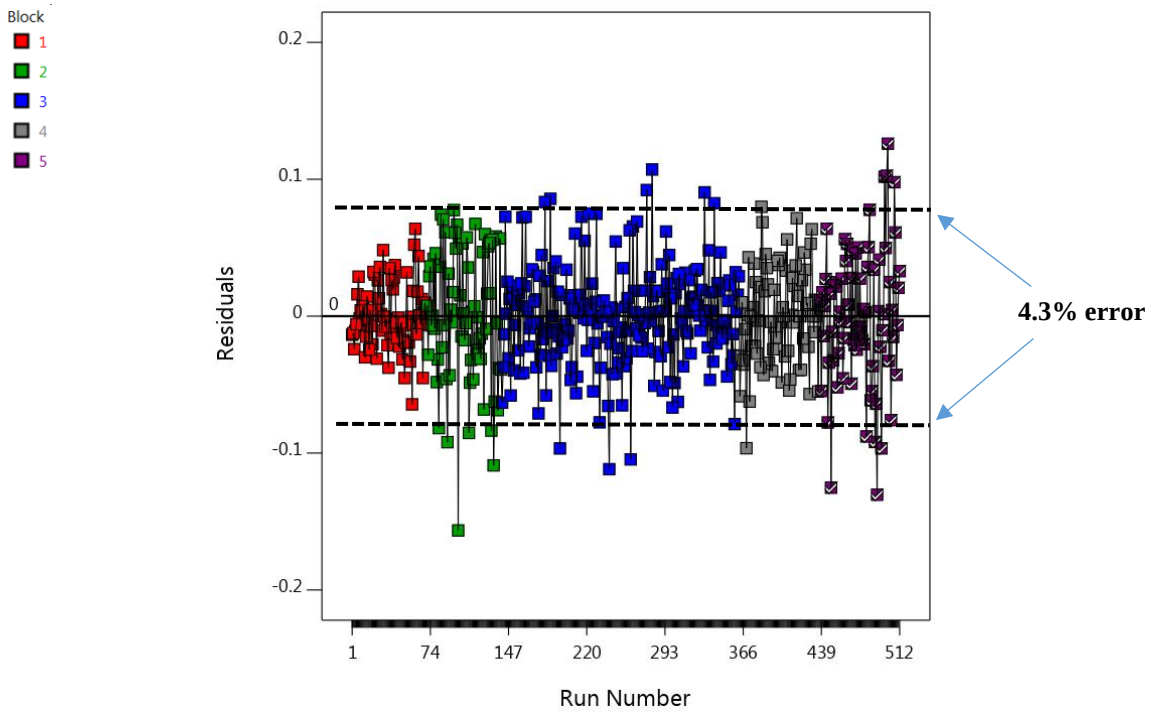

Figure 13. Residuals for CN model case-6, region R1, based on DOE blocks 1-4.

Although prediction errors with the current model and region R1 data are less than 5% (an adequate level) it is likely an investigator would pursue a split region test to assess the possibility of achieving the more desirable 3% level. For the RAM development study, a split region test is simply based on breaking the angle-of-attack range into low and high alpha regions labeled as R2 and R3, shown in Fig. 8. For this study, the splitting process was arbitrarily continued until the seven regions in Fig. 8 were acquired. In an automated RAM progression, the splitting process would stop when models achieve the user specified fidelity level in terms of prediction error. Tables 5-6 show the resulting progression of prediction error as the regions are split and models are identified for normal force and pitching moment, respectively. For these cases, all regions were modeled with polynomials including some cubic and 3-factor interactions, and then tested against the target region's block-5 data to determine the level of prediction error.

Table 5. Normal force prediction error progression due to splitting

Region #	Passing Residual Error	Maximum Region C_N	Prediction Error
1	0.0759	1.7538	4.33%
2	0.0447	1.3262	3.37%
3	0.0487	1.7092	2.85%
4	0.0258	0.9897	2.61%
5	0.0322	1.3305	2.42%
6	0.0305	1.4660	2.08%
7	0.0321	1.6972	1.89%

In each table, regions R1-R7 are labeled (as identified in Fig. 8), the largest residual errors that pass the binomial test, and the maximum coefficient values are presented, along with the resulting prediction error. Models for normal force coefficient quickly achieve the desirable 3% level of prediction fidelity, whereas pitching moment is only within a 4% level after the same number of splits. This result may reflect the relatively more favorable signal-to-noise ratios for normal force.

Table 6. Pitching moment prediction error progression due to splitting

Region #	Passing Residual Error	Maximum Region C_m	Prediction Error
1	0.0602	1.0120	5.95%
2	0.0399	0.9137	4.36%
3	0.0454	1.0114	4.49%
4	0.0383	0.7520	5.09%
5	0.0485	0.9299	5.21%
6	0.0367	0.9612	3.82%
7	0.0337	1.0039	3.36%

C. Test Comparisons and Evaluations

Aerodynamic modeling results from conventional experiments, when used in simulation, are typically provided in the form of data look-up tables along with limited statistical information. The easiest comparisons to make between conventional measurements and the RAM polynomial models are in basic co-plots of the results. This comparison is shown in Fig. 14 for normal force and pitching moment with all control surfaces set to zero. The conventional data were selected from several repeated runs made under the same conditions as the designed experiments. Noted on the charts are the largest variations for the conventional data normalized by the maximum coefficient value under the range studied. As noted previously, normal force measurements exhibited greater signal-to-noise ratios compared to pitching moment, so a greater spread for repeatability of the pitching moment is expected. The results show the variability possible from day-to-day testing and explains the model convergence differences in Tables 5-6 found with normal force coefficient reaching the desired fidelity with less data.

Comparing aerodynamic model coefficients from both approaches was also accomplished by taking all the conventional OFAT data and fitting a large neural-net model so that surfaces from the two approaches could be compared and calculations of basic statistics could be computed. These results are shown in Table 7 and in Fig. 15. Table 7 highlights fit statistics of mean and standard deviation based on residuals corresponding to the CN and Cm models. OFAT-based models reflect a larger bias and standard errors compared to RAM-based polynomial models. Figure 15 shows a good match between the two model surfaces produced by the two models.

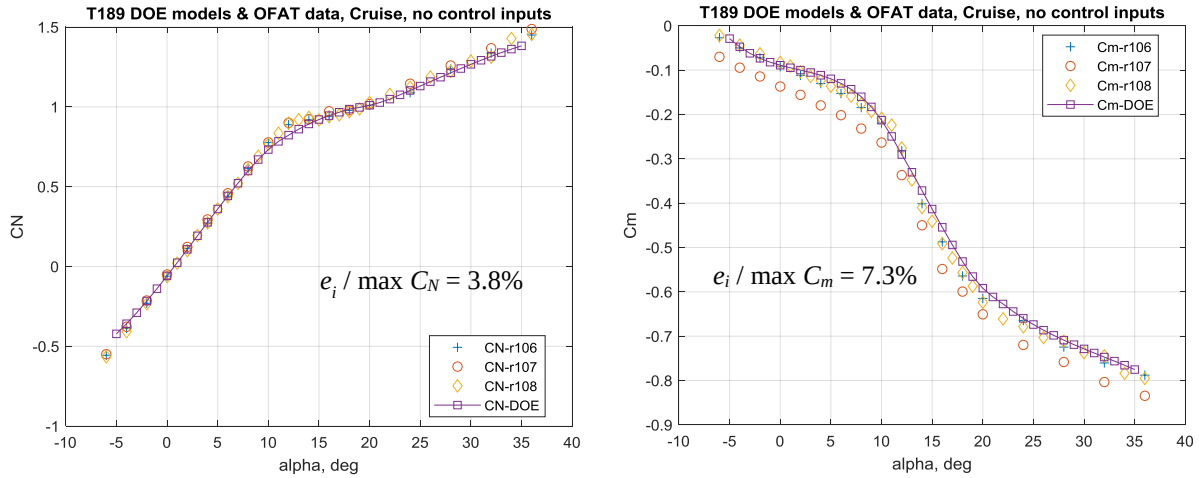

Figure 14. DOE and conventional longitudinal coefficients and largest measurement range.

Table 7. Improved statistics using RAM approach

Coefficient	Approach	Mean	Std. Error
CN	OFAT	0.057	0.114
“	RAM	0.001	0.051
Cm	OFAT	0.007	0.113
“	RAM	-0.007	0.046

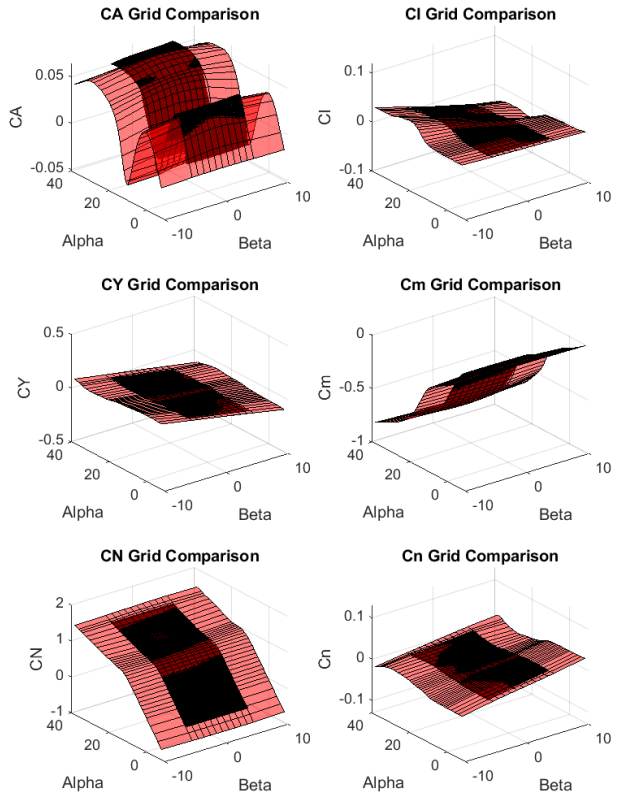

Figure 15. Comparison plots for OFAT data and resulting models from RAM-T test.

VI. Concluding Remarks

Motivated by UAM vehicle designs that present significant complexity and nonlinearity with possibilities for numerous factors and many unconventional factor interactions, a RAM approach is being developed. This study presents some preliminary results toward that goal. Designed experiments based on DOE, in an automated RAM process can provide statistical information before, during, and after the experiment is completed. This is extremely helpful to investigators working to obtain a specific desired level of model fidelity. A variety of statistical measures were presented and evaluated in this study. Each offers useful information throughout the entire process, however, prediction error evaluated on validation data is a clear primary metric for modeling under an automated RAM process.

Conventional testing was also performed with a primary purpose of developing aerodynamic models useful for flight dynamics simulation, design, and analysis. Comparing coefficient plots between the two approaches, conventional and RAM, are encouraging since both approaches represent the aerodynamic functions well. However, making comparisons of the two approaches in terms of time-to-test, quantity of data required, and utility of the final models is difficult. The two approaches have very different methodologies and in this study different test objectives. In general, the two approaches offer corroborating results with the benefit of more statistical control given to the RAM approach. The sequential nature of the RAM approach also inherently limits data collection to that required to match model complexity and fidelity requirements. In addition, for typical UAM vehicles where the number of factors may

be 2-4 times that of a conventional aircraft, an automated RAM approach provides guidance starting with experiment design, through test execution, and in final model analysis. Future work will refine and automate the RAM process.

Appendix

Additional aerodynamic data developed during the conventional experiment is provided to complete the modeling results. Figure A-1 shows the basic lateral-directional characteristics. The rolling moment plot indicates that the airplane rolls right at stall. Evident by the positive values of Cn_β, the aircraft is directionally stable, except for some very marginal instability after stall. The negative values of Cl_β indicate that the aircraft is laterally stable up to $\alpha = 36$ degrees.

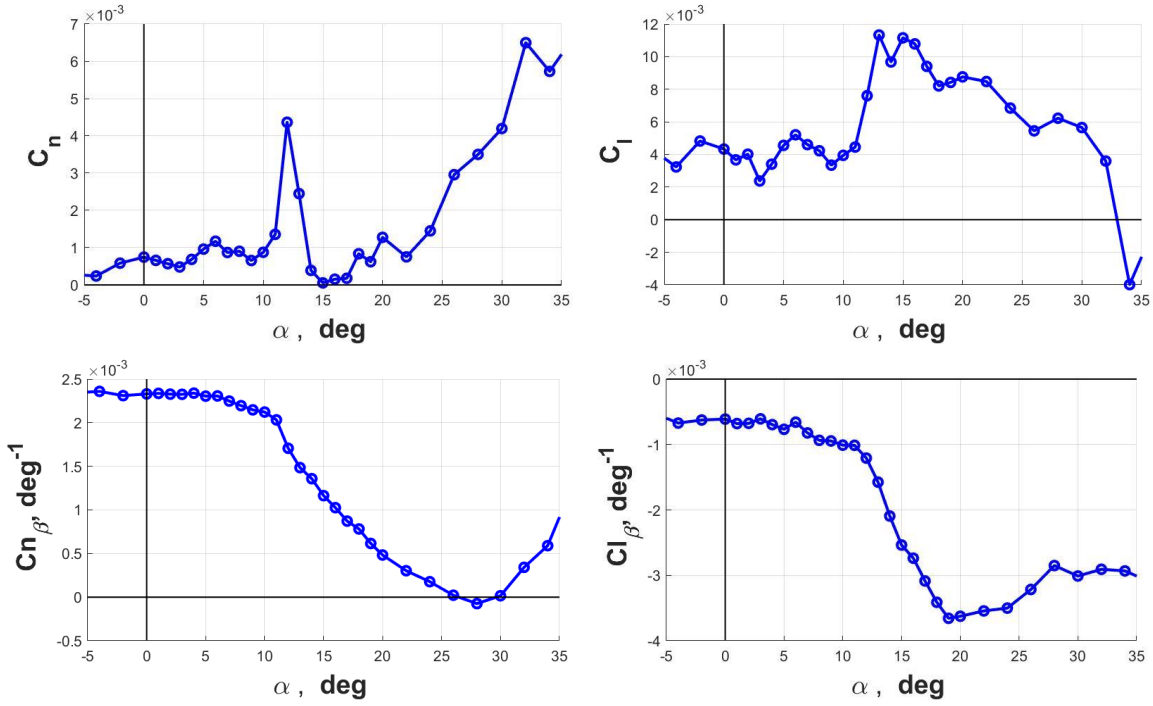

Figure A-1. Lateral-directional aerodynamics.

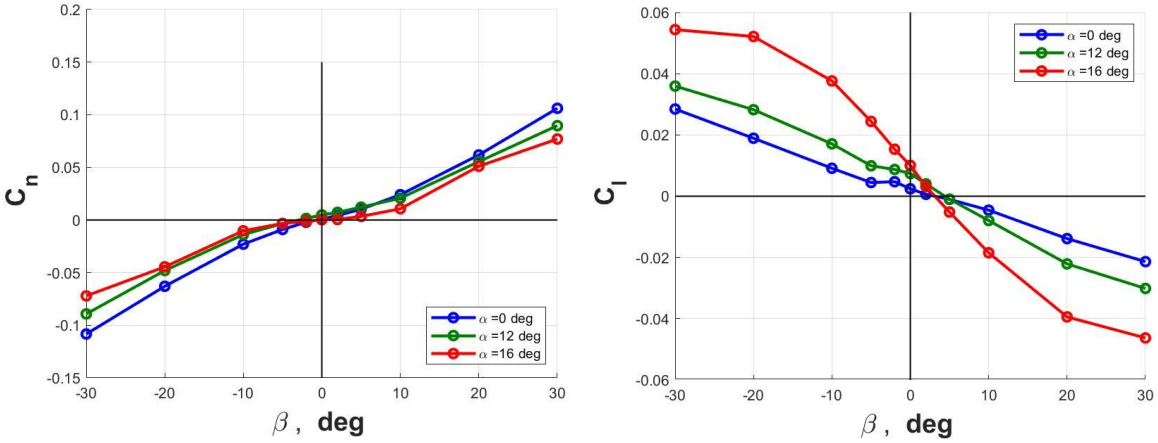

Figure A-2. Lateral-Directional Aerodynamics with Respect to Sideslip.

Figure A-2 shows the lateral-directional aerodynamics with respect to sideslip. Different angle-of-attack cases are shown. The lateral-directional aerodynamics present as largely conventional responses for this vehicle. There is no evidence of hysteresis effects or other nonlinear effects, even around stall, for the lateral-directional characteristics.

Plots of control power of the control surfaces are in Fig. A-3. The plots indicate that there is enough control surface power to overcome the rolling moments at stall. Lift and drag with respect to angle of attack are shown in Fig. A-4.

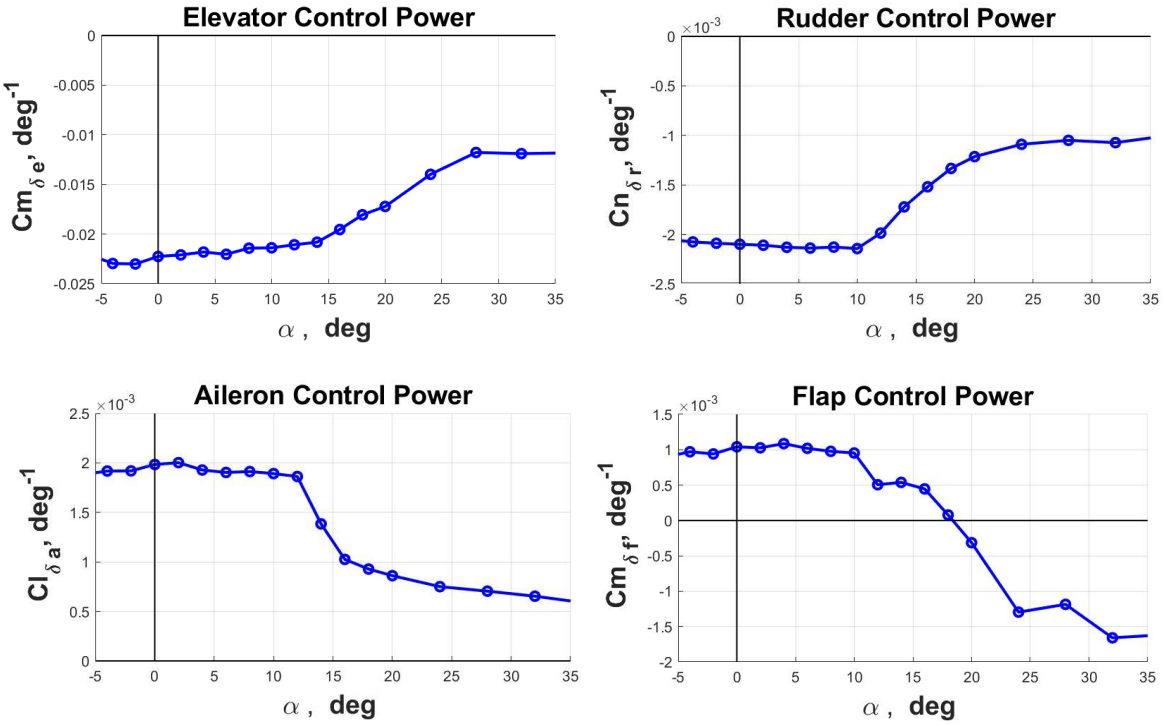

Figure A-3. Control power as a function of angle of attack.

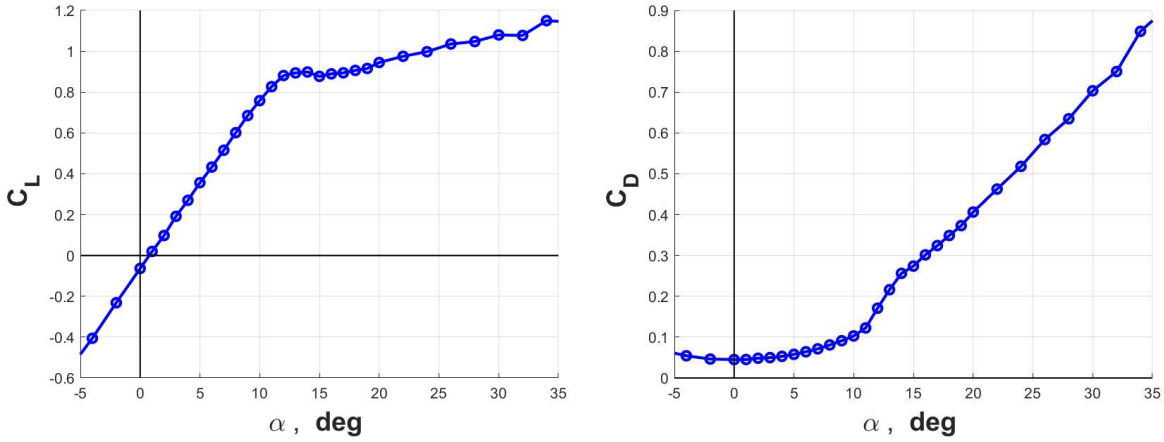

Figure A-4. Lift and drag with respect to angle of attack.

Acknowledgments

The authors extend their appreciation to the NASA Transformational Tools and Technologies Project.

References

[1] Booze Allen Hamilton, Final Report Urban Air Mobility (UAM) Market Study https://ntrs.nasa.gov/archive/nasa/casi.ntrs.nasa.gov/20190001472.pdf .

[2] Crown Consulting, Inc., McKinsey & Company, Ascension Global, Georgia Tech, Urban Air Mobility (UAM) Market Study, https://www.nasa.gov/sites/default/files/atoms/files/uam-market-study-executive-summary-v2.pdf .

[3] Button, Keith, "For Vahana, A Study in Coping with Complexity," Aerospace America, June 2019.

[4] De Loach, R., "Applications of Modern Experiment Design to Wind Tunnel Testing at NASA Langley Research Center," AIAA 98-0713, 36th AIAA Aerospace Sciences Meeting and Exhibit, Reno, NV, 1998.

[5] Morelli, E. A., and De Loach, R., "Ground Testing Results Using Modern Experiment Design and Multivariate Orthogonal Functions," AIAA 2003-0653, 41st AIAA Aerospace Sciences Meeting & Exhibit, Reno, NV, 2003.

[6] Landman, Drew, Simpson, Jim, Vicroy, Dan D., and Parker, Peter, "Response Surface Methods for Efficient Complex Aircraft Configuration Aerodynamic Characterization," Journal of Aircraft, Vol. 44, No. 4, July-August 2007.

[7] Landman, Drew, Simpson, Jim, Vicroy, Dan D., and Parker, Peter, "Hybrid Design for Aircraft Wind-Tunnel Testing Using Response Surface Methodologies," *Journal of Aircraft*, Vol. 44, No. 4, July-August 2007. DOI: 10.2514/1.25914.

[8] Landman, Drew, Simpson, Jim, Vicroy, Dan D., and Parker, Peter, "Response Surface Methods for Efficient Complex Aircraft Configuration Aerodynamic Characterization," *Journal of Aircraft*, Vol. 44, No. 4, July-August 2007. DOI: 10.2514/1.24810.

[9] Rothhaar, P., Murphy, P. C., Bacon, B. J., Grauer, J.; NASA Langley Distributed Propulsion VTOL Tilt Wing Aircraft Testing, Modeling, Simulation, Control, and Flight Test Development, AIAA AFM Conference, AIAA Aviation 2014, AIAA Paper No. 2014-2999.

[10] Busan, Ronald, Rothhaar, Paul, Croom, Mark, Murphy, Patrick C., Grafton, Sue, O'Neal, Anthony, "Enabling Advanced Wind-Tunnel Research Methods Using the NASA Langley 12-Foot Low Speed Tunnel," AIAA Aviation and Aeronautics Forum and Exposition 2014, AIAA Paper No. 2014-3000.

[11] Murphy, Patrick C. and Landman, Drew, "Experiment Design for Complex VTOL Aircraft with Distributed Propulsion and Tilt Wing," AIAA Atmospheric Flight Mechanics Conference, AIAA SciTech 2015, AIAA Paper No. 2015-0017.

[12] Murphy, Patrick C., Brandon, Jay, "Efficient Testing Combining Design of Experiment and Learn-to-Fly Strategies," AIAA SciTech Forum, Atmospheric Flight Mechanics Conference, AIAA 2017-0696, January, 2017. DOI: 10.2514/6.2017-0696.

[13] Simpson, James R. and Wisnowski, James W., "Streamlining Flight Test with the Design and Analysis of Experiments," Journal of Aircraft, Vol. 38, No. 6, November-December, 2001.

[14] Omran, Ashraf, Landman, Drew, Newman, Brett, "Global Stability and Control Derivative Modeling Using Design of Experiments," AIAA Flight Mechanics Conference, AIAA Paper No. 2009-5721, DOI: 10.2514/6.2009-5721.

[15] Brandon, Jay M., Morelli, Eugene A., "Nonlinear Aerodynamic Modeling From Flight Data Using Advanced Piloted Maneuvers and Fuzzy Logic," NASA/TM–2012-217778.

[16] Morelli, E. A., "Efficient Global Aerodynamic Modeling from Flight Data," 50th AIAA Aerospace Sciences Meeting, AIAA Paper 2012-1050, January, 2012.

[17] Brandon, J. M. and Morelli, E. A., "Real-Time Global Nonlinear Aerodynamic Modeling from Flight Data," Journal of Aircraft, Vol. 53, No. 5, September-October, 2016, pp. 1261-1297.

[18] Williams, Brianne, Y., Landman, Drew, Flory, Isaac L., and Murphy, Patrick C., "The Effect of Systematic Error in Forced Oscillation Testing," Aerospace Sciences Meeting, AIAA Paper No. 2012-0768.

[19] Cummings, R.M. and Schütte, A., "Integrated Computational/Experimental Approach to Unmanned Combat Air Vehicle Stability and Control Estimation", Journal of Aircraft, Vol. 49, No. 6 (2012), pp. 1542-1557. doi: 10.2514/1.C03143.

[20] Ghoreyshi Mehdi, Cummings, Russell M., "Unsteady Aerodynamics Modeling for Aircraft Maneuvers: a New Approach Using Time-Dependent surrogate Modeling," 30th AIAA Applied Aerodynamics Conference, AIAA 2012-3327, June, 2012.

[21] Murphy, P.C., Klein, V., Frink, Neal T., and Vicroy, Dan D., "System Identification Applied to Dynamic CFD Simulation and Wind-Tunnel Data," AIAA Atmospheric Flight Mechanics Conference, AIAA 2011-6522, August, 2011.

[22] Murphy, Patrick C., Klein, Vladislav, Frink, Neal T.: Nonlinear Unsteady Aerodynamic Modeling Using Wind Tunnel and Computational Data. Journal of Aircraft. Vol. 54: 659-683, No. 2, March-April 2017. DOI: 10.2514/1.C033881.

[23] Frink, Neal T., Murphy, Patrick C., Atkins, Harold L., Viken, Sally A., Petrilli, Justin L.: Computational Aerodynamic Modeling Tools for Aircraft Loss-of-Control. Journal of Guidance, Control, and Dynamics. Vol. 40: 789-803, No. 4, April 2017. DOI: 10.2514/1.G001736.

[24] Derlaga, Joseph M., and Buning, Pieter G., "Recent Progress in OVERFLOW Convergence Improvements," *to be published* at AIAA SciTech Forum, Jan. 2020.

[25] Buning, Pieter G., and Pulliam, Thomas H., "Near-Body Grid Adaption for Overset Grids," AIAA Paper 2016-3326, June 2016.

[26] Riddick, S. E., "An Overview of NASA's Learn-to-Fly Technology Development," AIAA Atmospheric Flight Mechanics Conference, AIAA SciTech Forum, January, 2020 (to be published).

[27] Morelli, E. A., "Autonomous Real-Time Global Aerodynamic Modeling in the Frequency Domain," AIAA Atmospheric Flight Mechanics Conference, AIAA SciTech Forum, January, 2020 (to be published).

[28] Weinstein, R., and Hubbard, J. E., "Global Aerodynamic Modeling using Automated Local Model Networks in Real Time," AIAA Atmospheric Flight Mechanics Conference, AIAA SciTech Forum, January, 2020 (to be published).

[29] Snyder, S. M., "Autopilot Design with Learn-to-Fly," AIAA Atmospheric Flight Mechanics Conference, AIAA SciTech Forum, January, 2020 (to be published).

[30] Scott, C., and Gonzalez, O. R., "On the Development of a Fuzzy Logic Model-less Aircraft Controller," AIAA Atmospheric Flight Mechanics Conference, AIAA SciTech Forum, January, 2020 (to be published).
[31] Fisher, Ronald A., "The Design of Experiments," 9th ed., Macmillan. ISBN 0-02-844690-9, 1971 (1935).
[32] Klein, Vladislav and Morelli, Eugene A., "Aircraft System Identification: Theory and Practice," 1st edition, AIAA Inc., Reston, Virginia, 2006.
[33] Montgomery, Douglas, C., "Design and Analysis of Experiments," 8th ed., Wiley, 2013.
[34] Box, G. E. P. and Wilson, K. B., "On the experimental attainment of optimum conditions," J. Roy. Statist. Soc., Ser. B Metho. Vol. 13, No. 1, pp. 1-45, 1951.
[35] De Loach, Richard, "Assessment of Response Surface Models Using Independent Confirmation Point Analysis," AIAA 2010-741, 48th AIAA Aerospace Sciences Meeting and Exhibit, Orlando, FL, 2010.